Optics & Laser Technology 175 (2024) 110733

Contents lists available at ScienceDirect

Optics and Laser Technology

journal homepage: www.elsevier.com/locate/optlastec

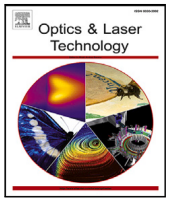

Full length article

Spatially distributed $\mathcal{PT}$ symmetric refractive index using four-wave-mixing in a double-Λ setup

Viačeslav Kudriašov [a], Wen-Te Liao [b,c,d,e], Gediminas Juzeliūnas [a], Hamid R. Hamedi [a,*]

[a] Institute of Theoretical Physics and Astronomy, Vilnius University, Saulėtekio 3, Vilnius LT-10257, Lithuania
[b] Department of Physics, National Central University, Taoyuan City 32001, Taiwan
[c] Physics Division, National Center for Theoretical Sciences, Taipei 10617, Taiwan
[d] Center for Quantum Technology, Hsinchu 30013, Taiwan
[e] Quantum Technology Center, National Central University, Taoyuan City 32001, Taiwan

ARTICLE INFO

Keywords:
Parity-time symmetry
Four-wave mixing
Double-Lambda atomic system

ABSTRACT

We propose a scheme for designing Parity-Time ($\mathcal{PT}$) spatially symmetric structures of the refractive index for a generated probe field propagating in a double-Λ (DL) atomic medium. By creating position-dependent atomic coherences and manipulating them controllably—via applied control fields and one-photon detuning—we achieve $\mathcal{PT}$ symmetry of the refractive index. This causes the refractive index components to become symmetric/antisymmetric functions of the transverse coordinate. We demonstrate that, in order to achieve $\mathcal{PT}$ condition for DL, a four-wave mixing process can be employed, with one of the control fields and detuning being anti-symmetric functions of the transverse coordinates, while the other control field being either symmetric or constant. Furthermore, we illustrate that this $\mathcal{PT}$ symmetry holds for different distances along the propagation direction and analyze its dependence on the phase matching conditions.

1. Introduction

Quantum mechanics relies heavily on the concept of the Hamiltonian H, which serves as a fundamental operator in determining the behavior of quantum systems. The Hamiltonian plays a critical role in dictating the system's energy spectrum and its time evolution which are essential characteristics of any quantum system. According to standard quantum mechanics, the Hamiltonian must satisfy the Hermitian condition to ensure that the energy spectrum is real, and the time evolution is unitary. However, several cases have been shown that certain non-Hermitian Hamiltonians can also exhibit completely real spectra, providing new insights into the behavior of quantum systems. Two examples of non-Hermitian Hamiltonians that can yield real spectra are the Bogoliubov-de Gennes equations [1,2] and the Schrodinger equation with a potential featuring a parabolic real part and a linear imaginary part [3].

Hermiticity is a sufficient, but not necessary condition for achieving an all-real spectrum for an operator. The spectrum of any Hermitian operator is purely real, but the opposite is not always true. Bender and Boettcher's seminal work [4] showed that a broad class of non-Hermitian Hamiltonians that are invariant under parity and time transformations, or $\mathcal{PT}$-symmetric, can display all-real spectra. Moreover, Bender and his colleagues introduced the concepts of unbroken and broken $\mathcal{PT}$ symmetry, highlighting the deep connection between $\mathcal{PT}$ symmetry and the reality of H's spectrum. The concept of $\mathcal{PT}$ symmetry has since extended to various branches of physics, including optics [5–9], atomic physics [10–15], acoustics [16,17], plasmonics [18,19], and electrical circuits [20].

Optics provides an ideal platform for realizing and experimentally testing $\mathcal{PT}$-related concepts due to the similarity between the Schrodinger equation and the Maxwell equation in the paraxial approximation. In optics, a medium's complex refractive-index, $n(x) = n_R(x) + in_I(x)$, with x representing a spatial coordinate, relates to the concept of the optical potential $V(x)$. The potential is $\mathcal{PT}$-symmetric when $V(x) = V^*(-x)$, implying that $n(x) = n^*(-x)$, with the real (imaginary) part being an even (odd) function of x, respectively.

Recent advancements in the development of optical materials with diverse functionalities have led to significant progress in $\mathcal{PT}$-symmetric optical theory [21,22]. A series of experiments have confirmed the theoretical results, utilizing various optical technologies such as synthetic photonic lattices [23,24], multi-level quantum systems [25–42], optical waveguides [43–45], optomechanical systems [46–50], acoustic crystals [51] and optical microcavities [52,53]. These studies have not only validated the theory, but also led to practical applications that are

* Corresponding author.
E-mail addresses: viaceslav.kudriasov@ff.vu.lt (V. Kudriašov), wente.liao@g.ncu.edu.tw (W.-T. Liao), gediminas.juzeliunas@tfai.vu.lt (G. Juzeliūnas), hamid.hamedi@tfai.vu.lt (H.R. Hamedi).

https://doi.org/10.1016/j.optlastec.2024.110733
Received 20 November 2023; Received in revised form 5 February 2024; Accepted 16 February 2024

highly attractive. Among these applications are unidirectional invisible light propagation [54–56], coherent perfect absorbers [57,58], giant light amplification [59] and novel lasers [60–62]. The potential of $\mathcal{PT}$-symmetric optical theory is vast, and its applications hold much promise for the future of optical devices. The advancements made thus far demonstrate the immense value of research in this field and highlight the exciting possibilities that lie ahead.

$\mathcal{PT}$-symmetric coherent atomic gases stand out among the different $\mathcal{PT}$-symmetric optical systems due to their distinctive attributes. Firstly, their refractive index maintains a true $\mathcal{PT}$-symmetric balance between gain and loss throughout the space. Secondly, they offer the advantage of being actively controllable and precisely manipulable *in situ* by adjusting system parameters. Thirdly, their inherent non-linearity, as they typically operate in resonance regimes between light and atoms, enhances the non-linear optical effects of $\mathcal{PT}$-symmetric optical systems.

Electromagnetically induced transparency (EIT) is a phenomenon in which a medium becomes transparent to light at a particular frequency range due to the interference of two or more light fields, typically a weak probe beam and a strong control beam [63]. This interference creates a "dark state" in the atomic medium, which inhibits absorption of the probe beam, rendering the medium transparent. $\mathcal{PT}$-symmetric systems, including $\mathcal{PT}$-symmetric atomic gases, can exhibit EIT. In such systems, the $\mathcal{PT}$ symmetry breaking can enhance or reduce EIT, depending on the specific system parameters. Therefore, $\mathcal{PT}$-symmetric systems can be used to control and manipulate EIT and can offer new possibilities for developing devices based on EIT [26,43,64].

In this paper, we propose a novel four-level double-Λ (DL) scheme for crafting $\mathcal{PT}$-symmetric refractive index profiles. Our approach leverages the four-wave-mixing (FWM) technique, departing from the direct utilization of EIT, as seen in prior scenarios [25–32,46]. This may extend its applicability to the atomic systems, where $\mathcal{PT}$-symmetry cannot be created inherently. In this case the DL system is driven by a pair of strong control fields with one probe field incident at the input. Once the second probe beam gets generated due to the FWM and a proper position-dependent control field or position-dependent detuning is used, a spatially dependent refractive index $n(x)$ fulfilling the $\mathcal{PT}$-symmetry condition for optical potential can be achieved. Indeed, the refractive index is related to the susceptibility of an atomic medium as $n = \sqrt{1+\chi} \approx 1 + \chi/2$ where both refractive index n and susceptibility χ are complex quantities. The optical susceptibility at some transition $i \leftrightarrow j$ relates directly to the coherence term of a density matrix $\chi \sim \rho_{ij}$. Creating a position dependent coherence $\rho_{ij}(x)$ through possible scenarios with suitable symmetry in the transverse coordinate x, the $\mathcal{PT}$ symmetry of the refractive index is seen to be achieved for the DL model. Accordingly, the real/imaginary parts of the separate refractive index components become symmetric/antisymmetric functions of the transverse coordinate [26]. By designing $\mathcal{PT}$-symmetric spatially distributed refractive index patterns, one can effectively generate optical potentials within the DL atomic medium. Below we consider possible scenarios where the $\mathcal{PT}$ condition can be achieved with the DL setup.

2. Model, theory and results

We consider an atom-light interaction setup with four energy levels comprising a DL configuration shown in Fig. 1. Each atom is characterized by two metastable ground states $|g\rangle$ and $|s\rangle$ and two excited states $|e_1\rangle$ and $|e_2\rangle$. This configuration is based on a mixture of two subsystems of Λ configuration. The medium is illuminated by a pair of probe fields and a pair of control fields. Each Λ component operates by using the coherent laser fields Ω_{c1} and Ω_{c2} to regulate the transmission of probe fields Ω_{p1} and Ω_{p2} across the DL system. This, in turn, causes the resonant probe beams to become transparent as a result of the destructive quantum interference [65].

Let us commence with formulating the fundamental equations that elucidate the interplay between optical fields and DL atoms. To simplify

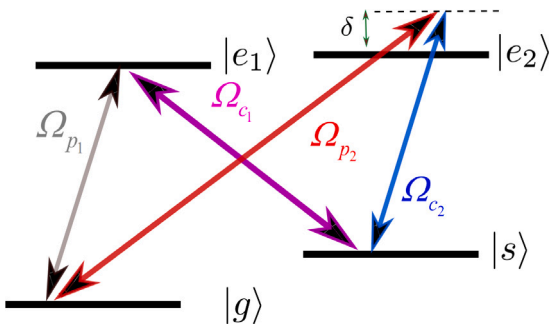

Fig. 1. Schematic representation of the four-level DL atom-light coupling configuration.

the analysis, we shall overlook the motion of the atomic center-of-mass. Furthermore, we assume that the strength of the probe fields Ω_{p_1} and Ω_{p_2} is significantly lower than that of the control fields Ω_{c_1} and Ω_{c_2}. Therefore, all atoms will persist in the ground state $|g\rangle$, and we can consider the impact of the probe fields as a perturbation while deducing the following equations [66], for the transitions $|e_1\rangle \leftrightarrow |g\rangle$ and $|e_2\rangle \leftrightarrow |g\rangle$

$$\dot{\rho}_{e_1g} = -\frac{\gamma_{e_1}}{2}\rho_{e_1g} + \frac{i}{2}\Omega_{c_1}\rho_{sg} + \frac{i}{2}\Omega_{p_1}, \tag{1}$$

$$\dot{\rho}_{e_2g} = \left(i\delta - \frac{\gamma_{e_2}}{2}\right)\rho_{e_2g} + \frac{i}{2}\Omega_{c_2}\rho_{sg} + \frac{i}{2}\Omega_{p_2}, \tag{2}$$

$$\dot{\rho}_{sg} = \frac{i}{2}\Omega^*_{c_1}\rho_{e_1g} + \frac{i}{2}\Omega^*_{c_2}\rho_{e_2g}, \tag{3}$$

where the one-photon detuning between the frequencies of the driving transition and the $|s\rangle \leftrightarrow |e_2\rangle$ transition is represented by $\delta = \omega_{c2} - \omega_{se_2}$, where ω_{c2},ω_{se_2} are the frequency of the driving field and the $|s\rangle \leftrightarrow |e_2\rangle$ transition. Considering decay rates for the excited states $|e_1\rangle$ and $|e_2\rangle$ to be equal $\gamma_{e_1} = \gamma_{e_2} = \Gamma$, the steady-state equations for the coherence terms can be rewritten as

$$\rho_{e_1g} = \frac{\Omega_{p_2}\Omega_{c_1}\Omega^*_{c_2} - \Omega_{p_1}|\Omega_{c_2}|^2}{2\delta|\Omega_{c_1}|^2 + i\Gamma|\Omega|^2}, \tag{4}$$

$$\rho_{e_2g} = \frac{\Omega_{p_1}\Omega_{c_2}\Omega^*_{c_1} - \Omega_{p_2}|\Omega_{c_1}|^2}{2\delta|\Omega_{c_1}|^2 + i\Gamma|\Omega|^2}, \tag{5}$$

where Ω is the total Rabi frequency of the control fields and $|\Omega|^2 = |\Omega_{c_1}|^2 + |\Omega_{c_2}|^2$. Using the equations for the coherence terms and assuming the second probe field is zero at the medium's entrance ($\Omega_{p_2}(z = 0) = 0$), the equations for both probe fields during their propagation read [66]

$$\Omega_{p_1}(z) = \frac{\Omega_{p_1 0}}{|\Omega|^2}\left[|\Omega_{c_1}|^2 + |\Omega_{c_2}|^2 \exp\left(-i\frac{\alpha z}{2Ld}\right)\right], \tag{6}$$

$$\Omega_{p_2}(z) = \frac{\Omega_{p_1 0}}{|\Omega|^2}\Omega^*_{c_1}\Omega_{c_2}\left[1 - \exp\left(-i\frac{\alpha z}{2Ld}\right)\right], \tag{7}$$

where $d = i + 2\delta|\Omega_{c_1}|^2/\left(\Gamma|\Omega|^2\right)$, $\Omega_{p_1 0} = \Omega_{p_1}(0)$ represents the incident probe beam, α is the optical depth of both the first and second probe fields, and L describes the optical length of the medium. For a given optical depth α it has been shown that there is an optimal value of one-photon detuning δ when the second probe field has the biggest intensity [66]. After substituting Eqs. (6), (7) to (4), (5) we obtain the z-dependent coherence terms in DL with FWM

$$\rho_{e_1g}(z) = -\Omega_{p_1 0}\frac{|\Omega_{c_2}|^2}{2\delta|\Omega_{c_1}|^2 + i\Gamma|\Omega|^2}\exp\left(-i\frac{\alpha z}{2Ld}\right), \tag{8}$$

$$\rho_{e_2g}(z) = \Omega_{p_1 0}\frac{\Omega^*_{c_1}\Omega_{c_2}}{2\delta|\Omega_{c_1}|^2 + i\Gamma|\Omega|^2}\exp\left(-i\frac{\alpha z}{2Ld}\right). \tag{9}$$

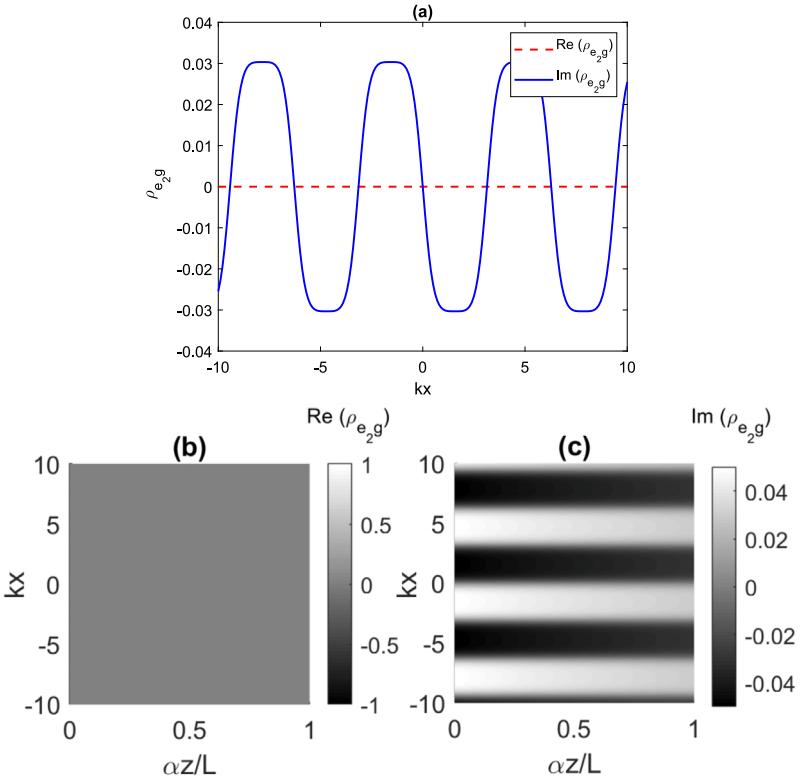

Fig. 2. (a): Plot for the real and imaginary parts of the coherence term $\rho_{e_2g}(x,z)$ at $\alpha z = L$. (b) and (c): 2D plots of the real and imaginary parts of $\rho_{e_2g}(x,z)$ for continuous z. Here, $\Omega_{c_1}(x) = \Omega_{c_10}\sin(kx)$, $\Omega_{c_2}(x) = \Gamma$, $\Omega_{c_10} = \Gamma$, $\Omega_{p_10} = 0.1\Gamma$, and $\delta = 0$.

To analyze the $\mathcal{PT}$ symmetry for the DL setup, we consider a general case with the control field and one-photon detuning being one-dimensional functions of the transverse coordinate, i.e. $\Omega(x)$ and $\delta(x)$. Then, it follows from Eq. (9) that the coherence term for $e_2 \leftrightarrow g$ optical transition (proportional to the refractive index $n(x)$ for this transition)

$$\rho_{e_2g}(x,z) = \Omega_{p_10}\frac{\Omega_{c_1}^*(x)\Omega_{c_2}(x)}{2\delta(x)|\Omega_{c_1}(x)|^2 + i\Gamma|\Omega(x)|^2}\exp\left(-\frac{i\alpha z}{2Ld(x)}\right) \tag{10}$$

and, likewise

$$\rho_{e_2g}^*(-x,z) = \Omega_{p_10}\frac{\Omega_{c_1}(-x)\Omega_{c_2}^*(-x)}{2\delta^*(-x)|\Omega_{c_1}(-x)|^2 - i\Gamma|\Omega(-x)|^2}\exp\left(\frac{i\alpha z}{2Ld^*(-x)}\right), \tag{11}$$

with the transverse coordinate dependence explicitly denoted. Equating both sides of $\rho_{e_2g}(x,z)$ and $\rho_{e_2g}^*(-x,z)$ provides the situation for the $\mathcal{PT}$ symmetry:

$$\frac{\Omega_{c_1}^*(x)\Omega_{c_2}(x)}{\Omega_{c_1}(-x)\Omega_{c_2}^*(-x)} = \frac{2\delta(x)|\Omega_{c_1}(x)|^2 + i\Gamma|\Omega(x)|^2}{2\delta^*(-x)|\Omega_{c_1}(-x)|^2 - i\Gamma|\Omega(-x)|^2} \times \exp\left[\frac{i\alpha z}{2L}\left(\frac{1}{d(x)} + \frac{1}{d^*(-x)}\right)\right]. \tag{12}$$

Let us now explore the scenarios in which this $\mathcal{PT}$ condition can be fulfilled, considering $\Omega(x)$ to be a real quantity which is even/odd function with respect to x. Specifically, we will investigate two cases: one with zero detuning $\delta = 0$ and another with non-zero position-dependent detuning. First, we consider the simpler case of no detuning, $\delta = 0$. This results in a position-independent quantity $d = i$, leading to $\frac{1}{d(x)} + \frac{1}{d^*(-x)} = 0$. In this case, the $\mathcal{PT}$ condition (12) simplifies to

$$\frac{\Omega_{c_1}(x)\Omega_{c_2}(x)}{\Omega_{c_1}(-x)\Omega_{c_2}(-x)} = -\frac{|\Omega(x)|^2}{|\Omega(-x)|^2} = -1, \tag{13}$$

where $|\Omega(-x)|^2 = |\Omega_{c_1}(-x)|^2 + |\Omega_{c_2}(-x)|^2 = |\Omega(x)|^2$. Here, we observe that the $\mathcal{PT}$ symmetry can be satisfied when one of the control fields, say Ω_{c_1}, is an odd function, implying $\Omega_{c_1}(-x) = -\Omega_{c_1}(x)$. Simultaneously, the other control field, Ω_{c_2}, can either be an even function or a constant, such as $\Omega_{c_2}(x) = \Omega_{c_2}(-x)$ or $\Omega_{c_2}(x) = \Omega_{c_20}$. Practically, achieving this condition becomes feasible when one of the control fields exhibits a linear variation with respect to the coordinate x, like $\Omega_{c_1}(x) \sim x$, or represents a harmonic function in the transverse coordinate x, for example, $\Omega_{c_1}(x) \sim \sin(kx)$ (e.g., a standing wave).

Fig. 2 illustrates the behavior of the coherence, $\rho_{e_2g}(x,z)$, in an atomic system subjected to a position-dependent control field $\Omega_{c_1}(x) = \Omega_{c_10}\sin(kx)$ and a constant Ω_{c_2}, with zero detuning. This coherence characterizes the response of atomic system to the generated probe field and provides valuable insights into the $\mathcal{PT}$ symmetry of the DL system. The calculations in the plot were conducted using the following parameter values: $\Omega_{p_10} = 0.1\Gamma, \Omega_{c_2} = \Gamma$, and $\delta = 0$. Here, z and x represent continuous spatial coordinates, and all parameters are scaled with the decay rate Γ. In this specific scenario, the coherence $\rho_{e_2g}(x,z)$ takes a purely imaginary value, given by the expression:

$$\rho_{e_2g}(x,z) = \Omega_{p_10}\frac{-i\Omega_{c_1}(x)\Omega_{c_2}}{\Gamma|\Omega(x)|^2}\exp\left(-\frac{\alpha z}{2L}\right). \tag{14}$$

As the plot on the panel (a) of Fig. 2 indicates, the behavior of ρ_{e_2g} at the end of the atomic medium ($\alpha z = L$) demonstrates that the spatially dependent control field Ω_{c_1} leads the imaginary part of the probe susceptibility as an odd function with periodic resonant oscillations. In this way, the atom undergoes oscillations in a periodic pattern

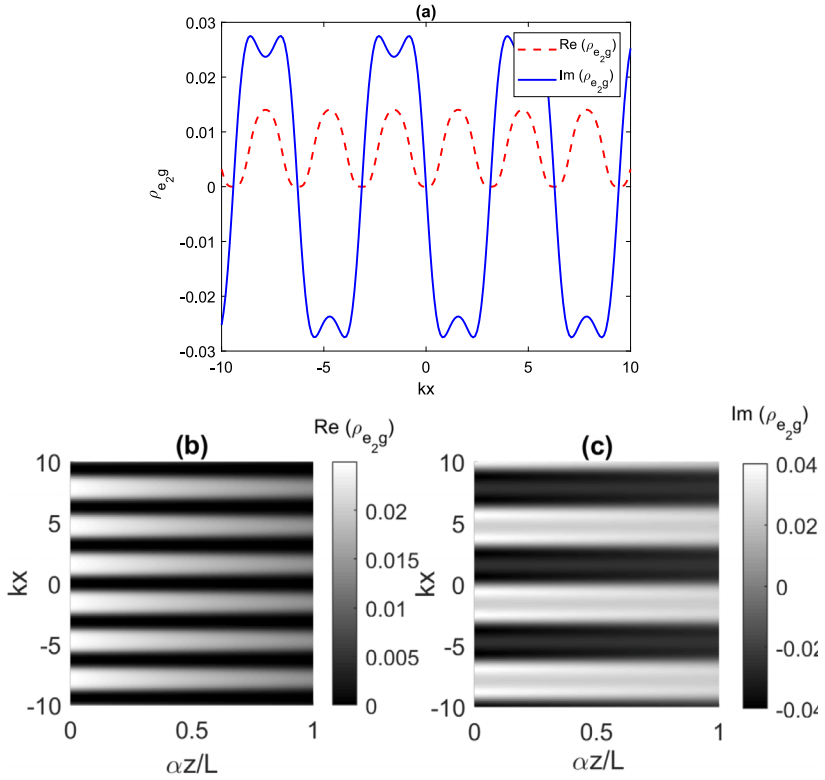

Fig. 3. (a): Plot for the real and imaginary parts of the coherence term $\rho_{e_2g}(x,z)$ at $\alpha z = L$. (b) and (c): 2D plots of the real and imaginary parts of $\rho_{e_2g}(x,z)$ for continuous z. Here, $\delta = \delta_0 \sin(kx)$ ($\delta_0 = \Gamma$) and $\Omega_{c_1}(x) = \Omega_{c_1 0}\sin(kx)$ ($\Omega_{c_1 0} = \Gamma$), and other parameters are the same as in Fig. 2.

across space, switching between regions of gain and loss. Notably, the dispersion (real part of susceptibility) remains constant and unaffected by the spatial variation of the control field (exhibiting an even function behavior). The 2D plots presented in Fig. 2(b) and (c) exhibit the propagation of the real and imaginary parts of $\rho_{e_2g}(x,z)$ in the medium. As the probe beam travels deeper into the medium, the modulation of loss and gain regions in the DL system causes small distortions in the $\mathcal{PT}$ symmetry patterns. However, the overall trend of $\mathcal{PT}$ symmetry remains intact.

Next, we delve into a more generalized scenario of non-zero detuning that satisfies the $\mathcal{PT}$ symmetry condition. Clearly, for a real anti-symmetric detuning function $\delta(-x) = -\delta(x)$, one gets $d^*(-x) = -d(x)$, leading to the convenient relation $\frac{1}{d(x)} + \frac{1}{d^*(-x)} = 0$. This simplifies Eq. (12) to

$$\frac{\Omega_{c_1}(x)\Omega_{c_2}(x)}{\Omega_{c_1}(-x)\Omega^*_{c_2}(-x)} = \frac{2\delta(x)|\Omega_{c_1}(x)|^2 + i\Gamma|\Omega(x)|^2}{2\delta(-x)|\Omega_{c_1}(-x)|^2 - i\Gamma|\Omega(-x)|^2} = -1, \tag{15}$$

and the $\mathcal{PT}$-symmetry condition holds true once again for any odd function Ω_{c_1} ($\Omega_{c_1}(-x) = -\Omega_{c_1}(x)$) and constant Ω_{c_2}, allowing to achieve a periodically modulated refractive index in space. Fig. 3(a) illustrates the real and imaginary components of ρ_{e_2g} for the control field $\Omega_{c_1}(x) = \Omega_{c_1 0}\sin(kx)$ and for the position-dependent detuning $\delta(x)$. To achieve experimental control of the position-dependent detuning, one can consider an in-phase spatial modulation to $\delta(x)$, akin to $\Omega_{c_1}(x)$, given by $\delta(x) = \delta_0 \sin(kx)$. This modulation can be realized through the AC Stark effect induced by an external periodic far-detuned CW laser field, causing corresponding energy level shifts of the state $|e_2\rangle$ [25,67]. For more details, we refer the interested readers to [25,68]. The periodic transverse modulation of one-photon detuning contributes to the spatial symmetry with periodic modulation in both the real and imaginary parts of the refractive index.

The plots in Fig. 3(a) show periodic patterns of loss and gain, which interestingly balance each other at both negative and positive spatial distances x, thereby giving rise to $\mathcal{PT}$ symmetry structures. The plots in panels (b) and (c) demonstrate the modification of $\mathcal{PT}$ symmetry patterns as the propagation distance z increases. As the probe beam travels through space, the oscillations exhibit a recurring pattern that alternates between regions of gain and loss. This indicates that the atom becomes localized at specific points of absorption or gain. Although the patterns may experience slight changes with the propagation distance, the overall $\mathcal{PT}$ symmetry remains invariant again.

Fig. 4 illustrates the $\mathcal{PT}$ symmetry patterns under non-zero detuning, varying $\Omega_{c_1 0}$ and δ_0. By setting $\Omega_{c_1 0} = 5\Gamma$ and $\delta_0 = 2\Gamma$, the spatial patterns exhibit more distinct, localized oscillations in a periodic fashion across space, alternating between gain and loss regions (see Fig. 4(a)). Remarkably, the $\mathcal{PT}$ symmetry persists. In comparison to Fig. 3(b,c), the $\mathcal{PT}$ symmetry patterns during propagation reveal significantly narrower structures for regions of absorption and gain.

The FWM process, as well known, exhibits the sensitivity to the phase mismatch [69,70]. To explore the impact of the phase mismatch on the $\mathcal{PT}$ symmetry in our setup, we assume all light beams are copropagating along the z direction. Then we can introduce a phase mismatch parameter, denoted as $\Delta_k = (k_{p_1} - k_{c_1} + k_{c_2} - k_{p_2})$, where k_{p_1}, k_{p_2}, k_{c_1} and k_{c_2} represent the wave-vectors of all involved light beams along the z axis. Note that the phase mismatch Δ_k can be reduced if one considers to vary the angle between beams in FWM process. Introducing the phase mismatch Δ_k into Maxwell equations describing the propagation of the probe fields, following the procedure given in [66], and taking $\Omega_{p_2}(0) = 0$, one gets the following relations

$$\Omega_{p_1}(z) = \frac{\Omega_{p_1 0}}{s_1 - s_2}\left[(q_1 - s_2)e^{s_1 z} + (s_1 - q_1)e^{s_2 z}\right], \tag{16}$$

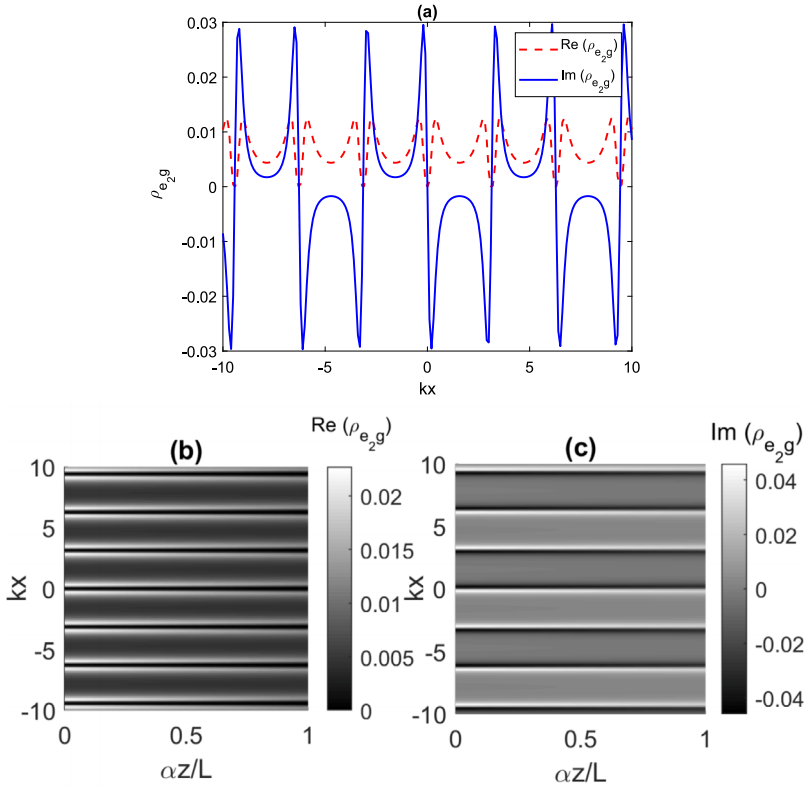

Fig. 4. (a): Plot for the real and imaginary parts of the coherence term $\rho_{e_2g}(x,z)$ at $\alpha z = L$. (b) and (c): 2D plots of the real and imaginary parts of $\rho_{e_2g}(x,z)$ for continuous z. Here, $\delta = \delta_0 \sin(kx)$ ($\delta_0 = 2\Gamma$) and $\Omega_{c_1}(x) = \Omega_{c_1 0}\sin(kx)$ ($\Omega_{c_1 0} = 5\Gamma$), and other parameters are the same as in Fig. 2.

$$\Omega_{p_2}(z) = \frac{\Omega_{p_1 0}}{q_2}\frac{s_1 - q_1}{s_1 - s_2}\left[(q_1 - s_2)e^{s_1 z} + (s_2 - q_1)e^{s_2 z}\right], \tag{17}$$

where parameters q_1, q_2, s_1, s_2 are expressed as

$$q_1(x) = -A(x)\frac{|\Omega_{c_2}|^2}{|\Omega(x)|^2}, \quad q_2(x) = A(x)\frac{\Omega_{c_1}(x)\Omega_{c_2}^*}{|\Omega(x)|^2}, \tag{18}$$

$$s_{1,2}(x) = \frac{1}{2}\left[-B(x) \pm \sqrt{B^2(x) + \frac{4A(x)\Delta_k|\Omega_{c_2}|^2}{i|\Omega(x)|^2}}\right], \tag{19}$$

and we introduced variables $A(x) = i\alpha/[2Ld(x)]$, $B(x) = A(x) + i\Delta_k$. Here, we explicitly denote that all parameters are dependent on the transverse coordinate x.

It can be seen that for $\Delta_k = 0$, Eqs. (16) and (17) reduce to Eqs. (6) and (7). Substituting Eqs. (16) and (17) into Eqs. (4), (5) we obtain the z-dependent coherence terms $\rho_{e_1g}(x,z)$ and $\rho_{e_2g}(x,z)$. Note, that the presence of phase mismatch Δ_k in the coherence terms makes their analytical expressions more complicated, so we use the numerical approach to conduct the $\mathcal{PT}$ symmetry patterns analysis. Fig. 5 illustrates simulations of $\rho_{e_2g}(x,z)$ at the end of the medium in the case where the phase mismatch is involved. One can see that in both cases, for zero $\delta(x) = 0$ and nonzero $\delta(x) = \delta_0 \sin(kx)$ detuning, as illustrated in panels (a) and (b), the imaginary part remains an odd function. However, the behavior of the real part is affected, compared to the previously considered phase matching cases. Indeed, one can easily see from the Fig. 5(a) that in the case of zero detuning the real part becomes also an odd function, breaking the $\mathcal{PT}$ symmetry. Although Fig. 5(b) may seem to be a better case, a closer look also shows a symmetry violation. One can see there are slight variations in the peak heights for the real part of $\rho_{e_2g}(x,z)$, indicating the deviation from a perfect $\mathcal{PT}$ symmetry. Thus, the analysis shows that the involvement of phase mismatch causes $\mathcal{PT}$ symmetry disruption, being particularly pronounced in the absence of detuning.

3. Concluding remarks

In summary, we developed an approach based on FWM in DL scheme to obtain spatially distributed refractive index $\mathcal{PT}$ symmetry patterns. Specifically, we derived Maxwell–Bloch equations for the DL system and obtained relations for the steady-state atomic coherences. Since the atomic coherences are position dependent (through the underlying dependencies of the control fields and detuning), by selecting the appropriate transverse coordinate symmetries of the control and detuning functions, conditions for the $\mathcal{PT}$ symmetry were obtained. In particular, we found that the $\mathcal{PT}$ symmetry can be realized when one of the control fields and detuning are odd function each, while another control field is either even or constant. The pattern symmetry retains stability during the FWM process remaining invariant at different propagation distances. It should be noted, however, that the symmetry holds only for the phase matching condition. Otherwise, in the case of phase mismatch, the real part of coherence acquires deviations leading to the disruption of $\mathcal{PT}$ symmetry.

The design of $\mathcal{PT}$-symmetric spatially distributed refractive index patterns enables the creation of optical potentials in the DL atomic medium, offering unprecedented control and manipulation of light propagation. The achieved $\mathcal{PT}$ symmetry holds promise for various applications, including compact integrated photonic devices, efficient sensors, and investigations into nonreciprocal light transport. Furthermore, this study significantly contributes to the broader understanding of $\mathcal{PT}$-symmetric systems and their potential applications in diverse physical and engineering disciplines.

A double-Λ (DL) configuration can be practically realized through experimental setups, such as employing ^{87}Rb atoms. This establishes a

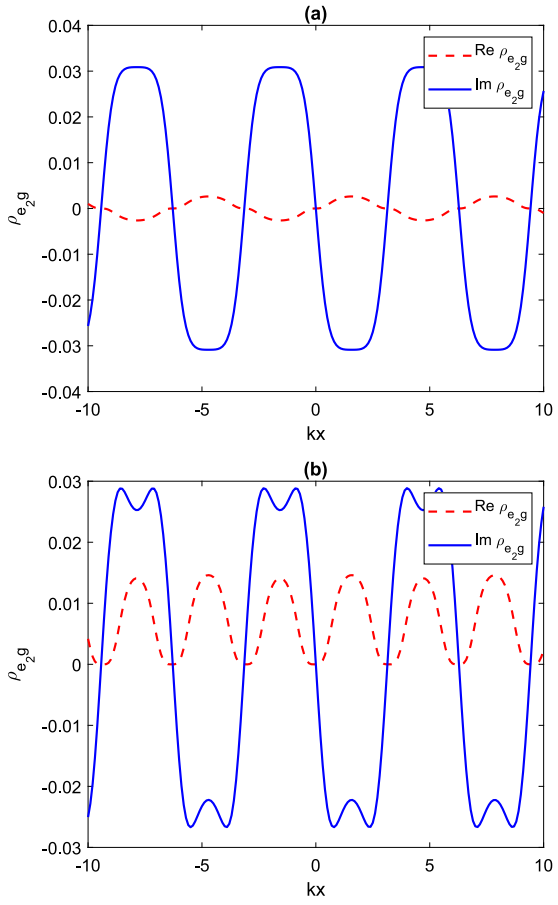

Fig. 5. Plots for the real and imaginary parts of the coherence term $\rho_{e_2g}(x,z)$ at $\alpha z = L$ for the cases (a) $\delta = 0$ and (b) $\delta = \delta_0 \sin(kx)$ when phase mismatch Δ_k is non-zero. Here, $\Omega_{c_1} = \Omega_{c_1 0} \sin(kx)$, $\Omega_{c_1 0} = \Gamma$, $\delta_0 = \Gamma$, and other parameters are the same as in Fig. 2.

DL level scheme, where the fundamental state $|g\rangle$ corresponds to the hyperfine state $|5S_{1/2}, F = 1, m_F = 0\rangle$. The lower state $|s\rangle$ is associated with the $|5S_{1/2}, F = 2, m_F = 0\rangle$ state. For the excited states, we can select $|e_1\rangle = |5P_{1/2}, F = 2, m_F = 1\rangle$ and $|e_2\rangle = |5P_{3/2}, F = 2, m_F = 1\rangle$.

CRediT authorship contribution statement

Viačeslav Kudriašov: Analysis and Investigation, Writing – original draft. **Wen-Te Liao:** Writing – review & editing, Formal analysis. **Gediminas Juzeliūnas:** Writing – review & editing, Funding acquisition, Conceptualization. **Hamid R. Hamedi:** Writing – review & editing, Supervision.

Declaration of competing interest

The authors declare that they have no known competing financial interests or personal relationships that could have appeared to influence the work reported in this paper.

Data availability

Data will be made available on request.

Acknowledgments

V. K, G. J and H. R. H acknowledge support from the Grant No. S-LLT-22-2 “Coherent Optical Control of Atomic Systems” by the Lithuanian Council of Research. W.-T. L. is supported by the National Science and Technology Council of Taiwan (Grant No. 110-2112-M-008-027-MY3, 110-2639-M-007 -001-ASP, 111-2923-M-008-004-MY3 \& 111-2639-M-007-001-ASP).

References

[1] N.N. Bogoliubov, J. Phys. USSR 11 (1947) 23.
[2] L. de Gennes, Superconductivity of Metals and Alloys, Benjamin, New York, 1966.
[3] T. Kato, Perturbation Theory for Linear Operators, 2nd ed., Springer, Berlin, 1995.
[4] S. Boettcher, C. Bender, Phys. Rev. Lett. 80 (1998) 5243.
[5] A. Ruschhaupt, F. Delgado, J. Muga, J. Phys. A: Adv. Phys.: X 779 38 (2005) L171.
[6] R. El-Ganainy, K. Makris, D. Christodoulides, Z. Musslimani, Opt. Lett. 32 (2007) 2632.
[7] K. Makris, R. El-Ganainy, D.N. Christodoulides, Z.H. Musslimani, Phys. Rev. Lett. 100 (2008) 103904.
[8] Z. Musslimani, K. Makris, R. El-Ganainy, D. Christodoulides, Phys. Rev. Lett. 100 (2008) 030402.
[9] C. Huang, F. Ye, Y. Kartashov, B. Malomed, X. Chen, Opt. Lett. 39 (2014) 5443.
[10] H. Cartarius, G. Wunner, Phys. Rev. A 86 (2012) 013612.
[11] D. Dast, D. Haag, H. Cartarius, G. Wunner, R. Eichler, J. Main, Fortschr. Phys. 61 (2013) 124.
[12] D. Dast, D. Haag, H. Cartarius, G. Wunner, J. Phys. A 46 (2013) 375301.
[13] E.-M. Graefe, U. Gunther, H. Korsch, A. Niederle, J. Phys. A 41 (2008) 255206.
[14] E.-M. Graefe, C. Liverani, J. Phys. A 46 (2013) 455201.
[15] E.-M. Graefe, H. Korsch, A. Niederle, Phys. Rev. Lett. 101 (2008) 150408.
[16] H. Jing, S. Ozdemir, X. Lu, J. Zhang, L. Yang, F. Nori, Phys. Rev. Lett. 113 (2014) 053604.
[17] X. Zhu, H. Ramezani, C. Shi, J. Zhu, X. Zhang, Phys. Rev. X 4 (2014) 031042.
[18] H. Benisty, A. Degiron, A. Lupu, A.D. Lustrac, S. Chenais, S. Forget, M. Besbes, G. Barbillon, A. Bruyant, S. Blaize, G. Lerondel, Opt. Express 19 (2011) 18004.
[19] A. Lupu, H. Benisty, A. Degiron, Opt. Express 21 (2013) 21651.
[20] J. Schindler, A. Li, M. Zheng, F. Ellis, T. Kottos, Phys. Rev. A 84 (2011) 040101, (R).
[21] Y. Lv, B. Yin, M. Gao, S. Liu, H. Li, M. Wang, S. Wu, Results Phys. 51 (2023) 106637.
[22] W.-C. Gao, C. Zheng, L. Liu, T.-J. Wang, C. Wang, Opt. Express 29 (2021) 517.
[23] A. Regensburger, C. Bersch, M.-A. Miri, G. Onishchukov, D. Christodoulides, U. Peschel, Nature 488 (2012) 167.
[24] M. Miri, A. Regensburger, U. Peschel, D. Christodoulides, Phys. Rev. A 86 (2012) 023807.
[25] C. Hang, G. Huang, V. Konotop, Phys. Rev. Lett. 110 (2013) 083604.
[26] J. Sheng, M. Miri, D.N. Christodoulides, M. Xiao, Phys. Rev. A 88 (2013) 041803, (R).
[27] C. Hang, D. Zezyulin, V. Konotop, G. Huang, Opt. Lett. 38 (2013) 4033.
[28] H.-J. Li, J. Dou, G. Huang, Opt. Express 21 (2013) 32053.
[29] C. Hang, D. Zezyulin, G. Huang, V. Konotop, B. Malomed, Opt. Lett. 39 (2014) 5387.
[30] C. Hang, G. Huang, Phys. Rev. A 91 (2015) 043833.
[31] Z. Zhang, Y. Zhang, J. Sheng, L. Yang, M. Miri, D. Christodoulides, B. He, Y. Zhang, M. Xiao, Phys. Rev. Lett. 117 (2016) 123601.
[32] P. Peng, W. Cao, C. Shen, W. Qu, J. Wen, L. Jiang, Y. Xiao, Nat. Phys. 12 (2016) 1139.
[33] Y. Ziauddin, L. Chuang, R.-K. Lee, Europhys. Lett. 115 (2016) 14005.
[34] S.-C. Tian, R.-G. Wan, L.-J. Wang, S.-L. Shu, H.-Y. Lu, X. Zhang, C.-Z. Tong, J.-L. Feng, M. Xiao, L.-J. Wang, Opt. Express 26 (2018) 32918.
[35] M. Abbas, A. Khurshid, I. Hussain, Ziauddin, Opt. Express 28 (2020) 8003.
[36] X. Wang, J.-H. Wu, Opt. Express 24 (2016) 4289.
[37] C. Hang, G. Huang, Adv. Phys.: X 2 (2017) 737.
[38] S.-L. Xu, H. Li, Q. Zhou, G.-P. Zhou, D. Zhao, M.R. Belic, J.-R. He, Y. Zhao, Opt. Express 28 (2020) 16322.
[39] R. Mukherjee, S. Konar, Chinese J. Phys. 74 (2021) 440.
[40] R. Mukherjee, S. Konar, J. Opt. 22 (2020) 105402.
[41] Y. Jiang, Y. Mei, Y. Zuo, Y. Zhai, J. Li, J. Wen, S. Du, Phys. Rev. Lett. 123 (2019) 193604.
[42] Z. Niu, Y. Jiang, J. Wen, C. Zhang, S. Du, I. Novikova, Appl. Phys. Lett. 124 (2024) 044005.
[43] A. Guo, G. Salamo, D. Duchesne, R. Morandotti, M. Volatier-Ravat, V. Aimez, G. Siviloglou, D. Christodoulides, Phys. Rev. Lett. 103 (2009) 093902.
[44] L. Feng, M. Ayache, J. Huang, Y.-L. Xu, M.-H. Lu, Y.-F. Chen, Y. Fainman, A. Scherer, Science 333 (2011) 729.

[45] Y. Qin, H. Chen, D. Luo, C. Pan, H. Hu, Y. Zhang, D. Wei, Opt. Express 29 (2021) 29175.
[46] X.Y. Zhang, Y.H. Zhou, Y.Q. Guo, X.X. Yi, Phys. Rev. A 98 (2018) 033832.
[47] H. Xiong, Y. Wu, Appl. Phys. Rev. 5 (2018) 031305.
[48] W. Li, Y. Jiang, C. Li, H. Song, Sci. Rep. 6 (2016) 31095.
[49] H. Jing, S.K. Ozdemir, Z. Geng, J. Zhang, X.-Y. Lu, B. Peng, L. Yang, F. Nori, Sci. Rep. 5 (2015) 9663.
[50] M. Peng, H. Zhang, Q. Zhang, T.-X. Lu, I.M. Mirza, H. Jing, Phys. Rev. A 107 (2023) 033507.
[51] Y. Meng, S. Lin, B. j. Shi, B. Wei, L. Yang, B. Yan, Z. Zhu, X. Xi, Y. Wang, Y. Ge, S. q. Yuan, J. Chen, G.-G. Liu, H. x. Sun, H. Chen, Y. Yang, Z. Gao, Phys. Rev. Lett. 130 (2023) 026101.
[52] B. Peng, S. Ozdemir, F. Lei, F. Monifi, M. Gianfreda, G. Long, S. Fan, F. Nori, C. Bender, L. Yang, Nat. Phys. 10 (2014) 394.
[53] L. Chang, X. Jiang, S. Hua, C. Yang, J. Wen, L. Jiang, G. Li, G. Wang, M. Xiao, Nat. Photonics 8 (2014) 524.
[54] H. Ramezani, T. Kottos, R. El-Ganainy, D. Christodoulides, Phys. Rev. A 82 (2010) 043803.
[55] Z. Lin, H. Ramezani, T. Eichelkraut, T. Kottos, H. Cao, D. Christodoulides, Phys. Rev. Lett. 106 (2011) 213901.
[56] X. Zhu, L. Feng, P. Zhang, X. Yin, X. Zhang, Opt. Lett. 38 (2013) 2821.
[57] Y. Sun, W. Tan, H. Li, J. Li, H. Chen, Phys. Rev. Lett. 112 (2014) 143903.
[58] C. Hang, G. Huang, V. Konotop, New J. Phys. 18 (2016) 085003.
[59] V. Konotop, V. Shchesnovich, D. Zezyulin, Phys. Lett. A 376 (2012) 2750.
[60] H. Hodaei, M.-A. Miri, M. Heinrich, D. Christodoulides, M. Khajavikhan, Science 346 (2014) 975.
[61] L. Feng, Z. Wong, R. Ma, Y. Wang, X. Zhang, Science 346 (2014) 972.
[62] H. Hodaei, M.A. Miri, A.U. Hassan, W.E. Hayenga, M. Heinrich, D.N. Christodoulides, M. Khajavikhan, Opt. Lett. 40 (2015) 4955.
[63] M. Fleischhauer, A. Imamoglu, J. Marangos, Rev. Modern Phys. 77 (2005) 633.
[64] H.-J. Li, J.-P. Dou, G. Huang, Opt. Express 21 (2013) 32053.
[65] H. Shpaisman, A.D. Wilson-Gordon, H. Friedmann, Phys. Rev. A 71 (2005) 043812.
[66] H. Hamedi, J. Ruseckas, G. Juzeliunas, Phys. Rev. A 98 (2018) 013840.
[67] D. Ma, D. Yu, X.-D. Zhao, J. Qian1, Phys. Rev. A 99 (2019) 033826.
[68] G. Alber, W.T. Strunz, Phys. Rev. A 50 (1994) R3577.
[69] C.-K. Chiu, Y.-H. Chen, Y.-C. Chen, I.A. Yu, Y.-C. Chen, Y.-F. Chen, Phys. Rev. A 89 (2014) 023839.
[70] T. Shui, W.-X. Yang, M.-T. Cheng, R.-K. Lee, Opt. Express 30 (2022) 6284.